

RESEARCH ARTICLE

Modeling and simulation of different and representative engineering problems using Network Simulation Method

J. F. Sánchez-Pérez¹, F. Marín², J. L. Morales³, M. Cánovas⁴*, F. Alhama¹

1 Department of Applied Physics, Universidad Politécnica de Cartagena, Cartagena, Spain, **2** Department of Electrical Engineering, Universidad Politécnica de Cartagena, Cartagena, Spain, **3** Department of Structures and Construction, Universidad Politécnica de Cartagena, Cartagena, Spain, **4** Metallurgical and Mining Engineering Department, Universidad Católica del Norte, Antofagasta, Chile

✉ These authors contributed equally to this work.

* manuel.canovas@ucn.cl



Abstract

Mathematical models simulating different and representative engineering problem, atomic dry friction, the moving front problems and elastic and solid mechanics are presented in the form of a set of non-linear, coupled or not coupled differential equations. For different parameters values that influence the solution, the problem is numerically solved by the network method, which provides all the variables of the problems. Although the model is extremely sensitive to the above parameters, no assumptions are considered as regards the linearization of the variables. The design of the models, which are run on standard electrical circuit simulation software, is explained in detail. The network model results are compared with common numerical methods or experimental data, published in the scientific literature, to show the reliability of the model.

OPEN ACCESS

Citation: Sánchez-Pérez JF, Marín F, Morales JL, Cánovas M, Alhama F (2018) Modeling and simulation of different and representative engineering problems using Network Simulation Method. PLoS ONE 13(3): e0193828. <https://doi.org/10.1371/journal.pone.0193828>

Editor: Ming Dao, Massachusetts Institute of Technology, UNITED STATES

Received: October 30, 2017

Accepted: February 20, 2018

Published: March 8, 2018

Copyright: © 2018 Sánchez-Pérez et al. This is an open access article distributed under the terms of the [Creative Commons Attribution License](https://creativecommons.org/licenses/by/4.0/), which permits unrestricted use, distribution, and reproduction in any medium, provided the original author and source are credited.

Data Availability Statement: All relevant data are within the paper and its Supporting Information files.

Funding: The authors received no specific funding for this work.

Competing interests: The authors have declared that no competing interests exist.

1. Background

In the text of González-Fernández [1] can be found a detailed description of the fundamentals of the method and the first applications in different fields of science and engineering: electrochemical processes, transport through membranes, heat transfer, etc. After this date, the Network Simulation Method hereinafter (NSM), has been employed in new problems developing models not covered by a specific new text, so that the person concerned should refer to the specific scientific publications or doctoral theses in the research group ‘Simulation Networks’, from Universidad Politécnica de Cartagena (UPCT), or research groups working with this method at the Universities of Granada, Jaen and Murcia: [2–7]. In this regard it should be mentioned applications in the fields of fluid flow to transport (of mass or heat), inverse problem in heat transmission, magneto-hydrodynamic flow, mechanical vibrations, tribology, dry friction, membrane transport, elasticity, development of specific numerical calculation programs, etc.

NSM had already been successfully applied in various fields of engineering: heat transfer [7–11], electrochemical reactions [12,13], transport across membranes [14], inverse problems [15–18], ion transport, magneto-hydrodynamics [19], problems coupled flow and transport [17,20–22], and others [23–26]; all these works describe nonlinear transport processes. In

addition, recently, it has been employed in mechanics of deformable solids [27], and dry friction at the atomic level.

On the other hand, there have been various programs that use the NSM as a tool for numerical calculation: PRODASIM for designing simple fins [28], PROCCA-09 for design and optimization of thermal problems [29], FATSIM-A for simulating flow fluids with solute transport problems [30], FAHET for simulation of flow fluids with heat transfer problems [31], EPSNET_10 for simulation problems elasticity [32] and OXIPSIS_12 for simulating corrosion problems [33].

The equivalence between the physical problem and the network model is that both are governed by the same differential equations in finite difference in space, covering both the elementary cell volume or as to the boundary conditions. However, time remains continuous variable in the design model.

The formal approach, which is the basis for the development of the problems, is the 'Network Theory' of Peusner [34], in which his 'thermodynamics of networks' is supported. Network models are for Peusner an accurate representation of the mathematic characteristic of the processes described. Thus, the variables which characterized of the problem must satisfy Kirchhoff's laws and their relationships determine the corresponding circuit elements. However, in each individual process and once conjugate variables chosen, the information on which circuit elements involved in the network model and how they connect with each and other, is obtained from the mathematical model and not on considerations of physical type on the role playing these variables.

In summary, in network theory, the feasibility of a network model involves:

- The existence of an independent network of time
- The existence of a conserved quantity called flow associated with each branch, connecting nodes and obeys the Kirchhoff Current Law (KCL)
- The existence of a magnitude that satisfies criteria of uniqueness associated with each node, and obeys the Kirchhoff Voltage Law (KVL)

It is going to be showed different models of application of the method to different fields of engineering to be presented in the second section. In the third, the governing equations, and its transposition into network models in the fourth. Applications are going to be shown in the fifth section, concluding with the conclusions in the sixth.

2. Introduction

2.1 Dry friction between microscope tip and smooth surface at atomic-scale

This study will analyze the atomic scale dry friction phenomenon using models implemented by the network simulation method, namely the Frictional Force Microscope hereinafter (FFM), evolution of the Scanning Force Microscope hereinafter (SFM), increases research capacity of phenomena at the atomic scale, key issue for understanding the origin and nature of the fundamental laws of friction. The analysis of the behavior of these point contacts is done by a two-dimensional model of friction at the atomic scale. The response of the tip is the 'stick-slip' type [35].

After a detailed review of the literature a number of techniques and materials for analysis have been selected. The cases are:

- NaF (001): it is a surface with translational symmetry. In this case the FFM is used [36]
- Highly Oriented Pyrolytic Graphite hereinafter (HOPG) is well-defined structures sheets, often chemically stable. In this case an SFM and Lateral Friction Microscope hereinafter (LFM) are used [37]

- Graphite: the Atomic Friction Microscope hereinafter (AFM) is used [38]

2.2 Problems of moving front

In problems with phase transitions in matter, the Stefan problem is a particular kind of boundary problem, in which this phase boundary can move with time. The classical Stefan problem aims to describe the temperature distribution in a phase change of matter. These problems are known like ‘problems of moving front’ [39].

There are numerous problems of moving front, which mainly include the melting and solidification processes as well as the processes of oxidation at high temperature.

2.3 The elastic problem

Theory of Elasticity describes the response of a solid object to external forces [40]. The solution to this problem involves knowing the stresses, strains and displacements generated in the solid. The analysis results allow the engineer to make decisions on the validity or suitability of structures and/or machines. On the other hand, the elasticity theory equations are widely used in other fields of science and technology, such as the study of seismic wave propagation or biomechanical behavior.

3. The governing equations

3.1 Dry friction between atomic force microscope tip and smooth surface at atomic-scale

The AFM, SFM, FFM tip physical scheme on a surface model, Fig 1, considers one rigid sliding body connected by three springs (one for each spatial direction) to the mobile support. Each spring reflects the elastic interaction between the two surfaces during the contact [36,38]. The sliding body involves the interaction with the surface and the inertial effect.

Several forces act on the tip in x-direction: inertial force represented by ‘ $m \cdot (d^2x_t/dt^2)$ ’, where x_t is the absolute displacement of the tip of mass m ; elastic force from the spring, represented by the term ‘ $k_x \cdot (x_M - x_t)$ ’; and damping force represented by the term ‘ $c_x \cdot (dx_t/dt)$ ’. The coefficients of these forces are constants. In addition, the surface-tip interaction force is built from a surface potential [36–38]. Thus, the NaF surface with FFM tip potential, Hölscher et al. [36] is:

$$V(x_t, y_t) = V_0 \cdot \cos\left(\frac{2\pi}{a_x} \cdot x_t\right) \cdot \cos\left(\frac{2\pi}{a_y} \cdot y_t\right) \quad (1)$$

where the potential amplitude, V_0 , is 1 eV, while a_x and a_y , are 4.62 Å for both parameters. Hölscher et al. [37] use a slight modification of Eq (1) to study HOPG surface and a SFM tip:

$$V_{HOPG}(x_t, y_t) = -V_0 \cdot \left[2 \cdot \cos\left(\frac{2\pi}{a} \cdot x_t\right) \cdot \cos\left(\frac{2\pi}{a\sqrt{3}} \cdot y_t\right) + \cos\left(\frac{4\pi}{a\sqrt{3}} \cdot y_t\right) \right] \quad (2)$$

where V_0 is 0.5 eV and the lattice constant, a , is 2.46 Å.

Sasaki et al. [38] used the Lennard-Jones potential to study the graphite and an AFM tip:

$$V_{TS} = \sum_i 4\epsilon \cdot \left[\left(\frac{\sigma}{r_{0i}}\right)^{12} - \left(\frac{\sigma}{r_{0i}}\right)^6 \right] \quad (3)$$

where the strength of the potential, ϵ , is $0.87381 \cdot 10^{-2}$ eV, and the value of the distance between the tip and the surface atom at which the potential is zero, σ , is 2.4945 Å. The tip and the i -th

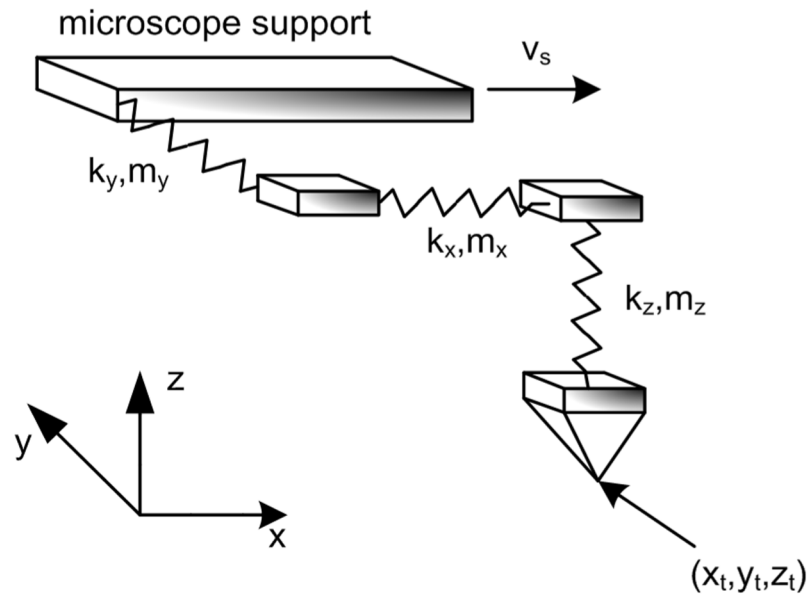


Fig 1. AFM, FFM and SFM tip model.

<https://doi.org/10.1371/journal.pone.0193828.g001>

atom of the surface distance, r_{0i} , is calculated from the i -th atom position inside the lattice, which is defined by its constant, 2.46 \AA , and the nearest distance between 2 carbon atoms, 1.42 \AA . Hölscher et al. employed the same potential with the same surface and microscope [41], but σ is equal to 3.4 \AA .

As a consequence of applying the balance of the tip forces, Fig 1, the equations could be written:

$$\begin{cases} m \cdot \ddot{x}_t = k_x \cdot (x_M - x_t) - \frac{\partial V}{\partial x_t} - c_x \cdot \dot{x}_t \\ m \cdot \ddot{y}_t = k_y \cdot (y_M - y_t) - \frac{\partial V}{\partial y_t} - c_y \cdot \dot{y}_t \\ m \cdot \ddot{z}_t = k_z \cdot (z_M - z_t) - \frac{\partial V}{\partial z_t} - c_z \cdot \dot{z}_t \end{cases} \quad (4)$$

The microscope movement is a set of trips in the x -direction.

3.2 Moving front problems

In moving front problems, there is increase, or decrease, of temperature, or a species, such as oxygen, increases its concentration. This depends on the process studied. The result is a new state or phase with different properties. Therefore, a new interface is generated. This interface is moved inside the structure producing the change of phase or state. Its position is represented as a distance function, Fig 2.

The problem considered has a semi-infinite structure, whose free surface, $x = 0$, is exposed to a constant concentration of oxygen or temperature, C_0 , [42,43]. These processes are almost instantaneous. Therefore, as soon as the temperature or the oxygen concentration reaches a determinate value, c_{cr} , at one point, solidification or melting, oxidation interface will move to that point. The process described is a moving boundary problem, whose governing equations

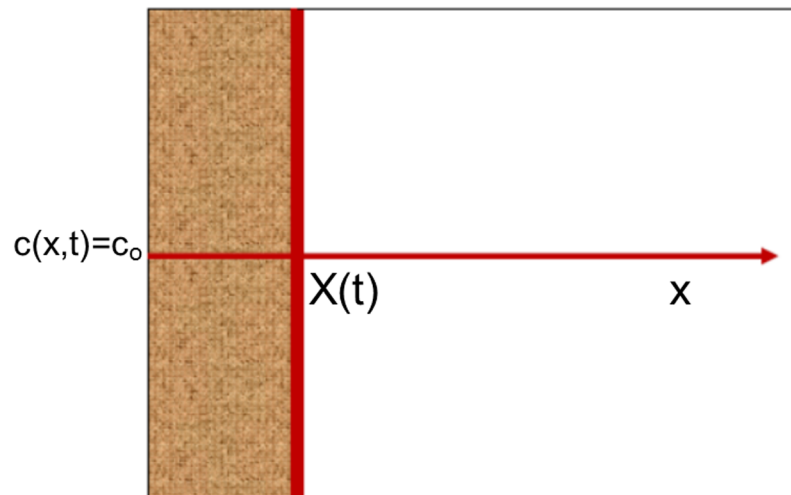


Fig 2. Scheme of areas within the metal, solid or liquid.

<https://doi.org/10.1371/journal.pone.0193828.g002>

are:

$$D_1 \frac{\partial^2 c_1(x, t)}{\partial x^2} = \frac{\partial c_1(x, t)}{\partial t}; \quad 0 < x < X(t) \quad (5)$$

$$D_2 \frac{\partial^2 c_2(x, t)}{\partial x^2} = \frac{\partial c_2(x, t)}{\partial t}; \quad X(t) < x < \infty \quad (6)$$

where D_1 and D_2 are the diffusivities of each phase. The initial and boundary conditions are:

$$X(0) = 0 \quad (7)$$

$$c_2(x, 0) = 0, \quad 0 < x < \infty \quad (8)$$

$$c_1(0, t) = c_0, \quad t > 0 \quad (9)$$

$$c_2(\infty, t) = 0, \quad t > 0 \quad (10)$$

The difference between flow values at the boundary between the two phases is responsible for the progress of the interface. Applying the conservation equation to concentrations [44,45], we have:

$$\phi_1(X) - \phi_2(X) = \Delta c \cdot \frac{dX}{dt} \quad (11)$$

where Δc is the oxygen concentration or temperature jump at the interface, and subscripts 1 and 2 refer to the oxide and metal phases or solid (or liquid and solid phase), respectively.

Eq (11) is called the Stefan condition. This equation can be written as:

$$-D_1 \frac{\partial c_1(x, t)}{\partial x} = -D_2 \frac{\partial c_2(x, t)}{\partial x} + \Delta c \cdot \frac{dX}{dt}, \quad t > 0 \quad (12)$$

3.3 Governing equation for the elastic problem

Navier's equation [40], as the governing equation, represents the equilibrium forces in terms of displacements \mathbf{u} for each point of the elastic body, Fig 3: λ

$$\mu \nabla^2 \mathbf{u} + (\lambda + \mu) \nabla(\nabla \cdot \mathbf{u}) + \mathbf{f} = \mathbf{0} \tag{13}$$

where \mathbf{f} is the volume force vector and λ, μ the material properties of the elastic body.

For 2D problems in Cartesian coordinates, Navier's equations are reduced to two coupled differential equations:

$$\left. \begin{aligned} \mu \nabla^2 u_x + (\lambda + \mu) \frac{\partial}{\partial x} \left(\frac{\partial u_x}{\partial x} + \frac{\partial u_y}{\partial y} \right) + f_x &= 0 \\ \mu \nabla^2 u_y + (\lambda + \mu) \frac{\partial}{\partial y} \left(\frac{\partial u_x}{\partial x} + \frac{\partial u_y}{\partial y} \right) + f_y &= 0 \end{aligned} \right\} \tag{14}$$

The required boundary conditions can be applied in displacements u_i^b or tractions terms t_i^b , Fig 3. The first condition is directly imposed, but the second required a complex relation by coupling of the first partial derivatives of the main unknowns and the outer normal vector of the boundary \mathbf{n} :

$$\left. \begin{aligned} t_x^b &= \left[\lambda \left(\frac{\partial u_x}{\partial x} + \frac{\partial u_y}{\partial y} \right) + 2\mu \frac{\partial u_x}{\partial x} \right] n_x + \mu \left(\frac{\partial u_x}{\partial y} + \frac{\partial u_y}{\partial x} \right) n_y \\ t_y^b &= \mu \left(\frac{\partial u_x}{\partial y} + \frac{\partial u_y}{\partial x} \right) n_x + \left[\lambda \left(\frac{\partial u_x}{\partial x} + \frac{\partial u_y}{\partial y} \right) + 2\mu \frac{\partial u_y}{\partial y} \right] n_y \end{aligned} \right\} \tag{15}$$

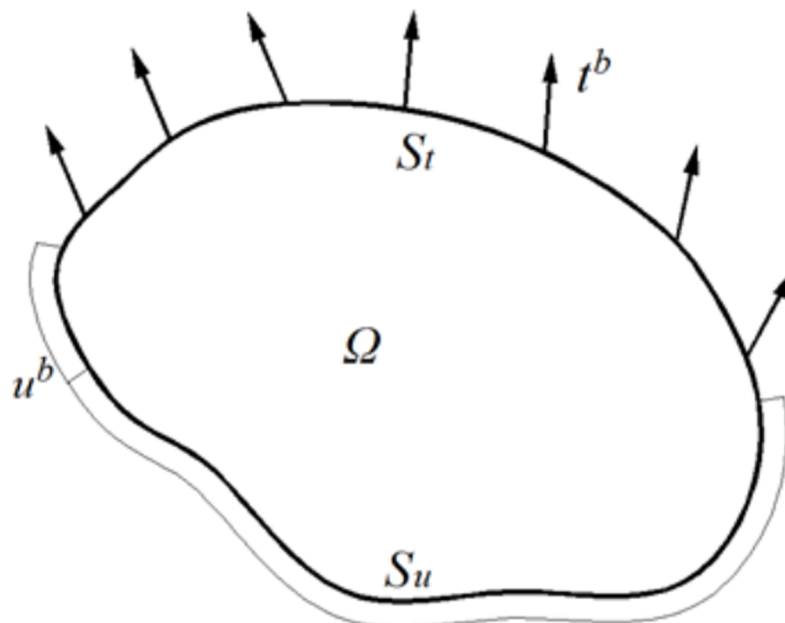


Fig 3. Elastic domain Ω under displacements u^b and tractions t^b boundary conditions defined over S_u and S_t respectively.

<https://doi.org/10.1371/journal.pone.0193828.g003>

Solved the elastic problem defined by Eq (14), the stress components can be evaluated from the displacement using the Lamé's equations:

$$\left. \begin{aligned} \sigma_{xx} &= \lambda \left(\frac{\partial u_x}{\partial x} + \frac{\partial u_y}{\partial y} \right) + 2\mu \frac{\partial u_x}{\partial x} \\ \sigma_{yy} &= \lambda \left(\frac{\partial u_x}{\partial x} + \frac{\partial u_y}{\partial y} \right) + 2\mu \frac{\partial u_y}{\partial y} \\ \sigma_{xy} &= \mu \left(\frac{\partial u_x}{\partial y} + \frac{\partial u_y}{\partial x} \right) \end{aligned} \right\} \quad (16)$$

4. Network models

4.1 Atomic force microscope simulation network models

The initial conditions related to displacements, $x_M - x_t = y_M - y_t = z_M - z_t = 0$, and velocities, $dx_t/dt = dy_t/dt = dz_t/dt = 0$, are inserted in the specifications of the capacitors initial conditions (initial voltage value) and of the coils (initial current value), respectively. The whole network model is now run employing PSpice [46,47].

The reliable network model design needs equivalence between the model and the process equations, including the initial conditions. Since Eq (4), the basic network model is corresponded with this equation, to which initial conditions must be added. Modeling basic rules are explained in González-Fernández [1]. The first is to select the equivalence between physical and electrical variables (different choices give rise to different networks). The following equivalence is established for the problem: x_t (tip displacement in the x-direction) \equiv q (electric charge in the network), or dx_t/dt (tip velocity in the x-direction) \equiv $dq/dt = i$ (electric current at the network). In the other directions, similar equivalences are applied.

Now, each addend of the Eq (4) is represented by an electric potential difference in a circuit element whose constitutive equation is analogous to the addend. Hence, the second Kirchhoff's law application on a network equivalent to the equation allows us to solve the equation. The addend of Eq (4) ' d^2x_t/dt^2 ' is correlated with an inductance whose constitutive equation is $V_L = L(di/dt) = L(d^2q/dt^2)$, with $L = 1H$. Equally, the same electrical element is used for the remainder directions. The non-linear terms cannot be implemented directly, and must be defined by controlled sources or additional circuits. In the event of voltage or current source, their output is defined by a routine as an arbitrary formula of the dependent variables. The most text books do not consider this classical electrical analogy in this way, becoming the NSM more interesting and efficient in the field of numerical computation.

After the integration of ' dx_t/dt ', equivalent to the current in the main circuit, the term ' x_t ' is available. The integration is implemented using a secondary circuit in the models for NaF surface analyzed by FFM, Fig 4(b), for graphite surface analyzed by AFM, Fig 5(c). The terms ' y_t ' and ' z_t ' are implemented in similar network models. The secondary circuit is implemented by a controlled source, F_{1x} , which generates the current, ' dx_t/dt ', obtained from the voltage in an ammeter connected in series in the main circuit, V_x . A capacitor with $C_{x1} = C_{y1} = C_x = 1F$ is used to integrate the current of F_{1x} , and the voltage in this element, $V_{Cx1} = V_{Cy1} = V_{Cx} = C_x^{-1} \cdot \int (dx_t/dt) dt$, is simply the variable ' x_t '. A resistor with a very high value, R_{INF} , improves the algorithm stability.

Once the variable ' x_t ' has been determined, the addend ' $k_x(x_M - x_t)$ ' in the model for NaF surface analyzed by a FFM, is implemented by a voltage from a controlled source, E_2 . For graphite surface analyzed by an AFM, another controlled source, E_{Tx1} , provides the necessary voltage. The secondary circuit shown in Fig 4(c) provides the variable ' x_M ', the product of the constant velocity of the microscope support and time.

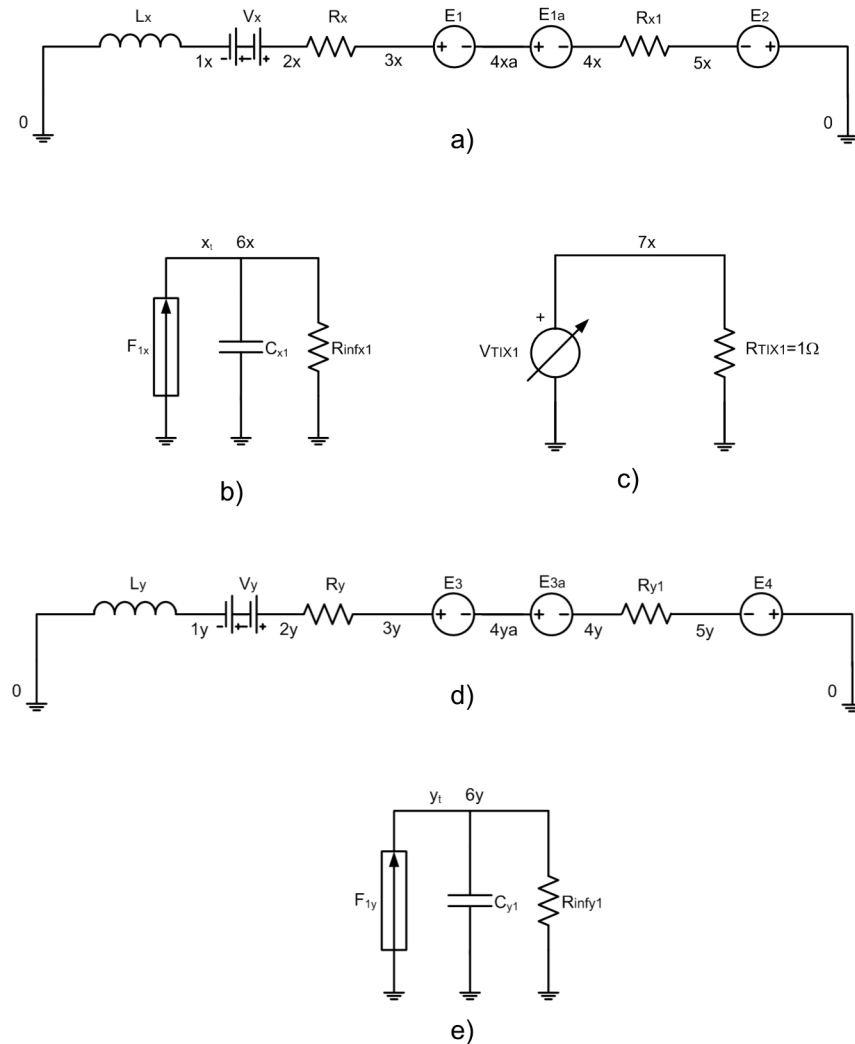


Fig 4. Network model of NaF with FFM and HOPG with SFM. a) and d) Main circuits, b) and e) secondary circuits to get x_t and y_t , and c) secondary circuit to the time.

<https://doi.org/10.1371/journal.pone.0193828.g004>

A pair of controlled sources, E_1 and E_{1a} , generates the voltage correspondent to ' $\partial V/\partial x_t$ ', for NaF surface analyzed by a FFM. For graphite surface analyzed by an AFM, the controlled source, E_{Tx2} , generates the voltage correspondent to potential gradient. The Lennard-Jones' potential, represented in the secondary circuit of Fig 5(b), is selected. The addends associated to $\partial V/\partial y_t$ and $\partial V/\partial z_t$ are implemented in a similar way. The last one of the first equation in Eq (4) is equivalent to a resistor, characterized by ' c_x ', in the models for NaF surface analyzed by a FFM. For the remainder equations in Eq (4), a similar form is implemented.

The initial conditions corresponding to displacements, $x_M - x_t = y_M - y_t = z_M - z_t = 0$, and velocities, $dx_t/dt = dy_t/dt = dz_t/dt = 0$, are implemented by the initial conditions in capacitors and coils, respectively. PSpice [46,47] allows us to simulate the network model.

4.2 Moving front simulation network models

The details of the general rules of the NSM, with applications to different types of problems, are explained in González-Fernández and Alhama [1]. However, for a better interpretation the following steps are described for the design of the network model.

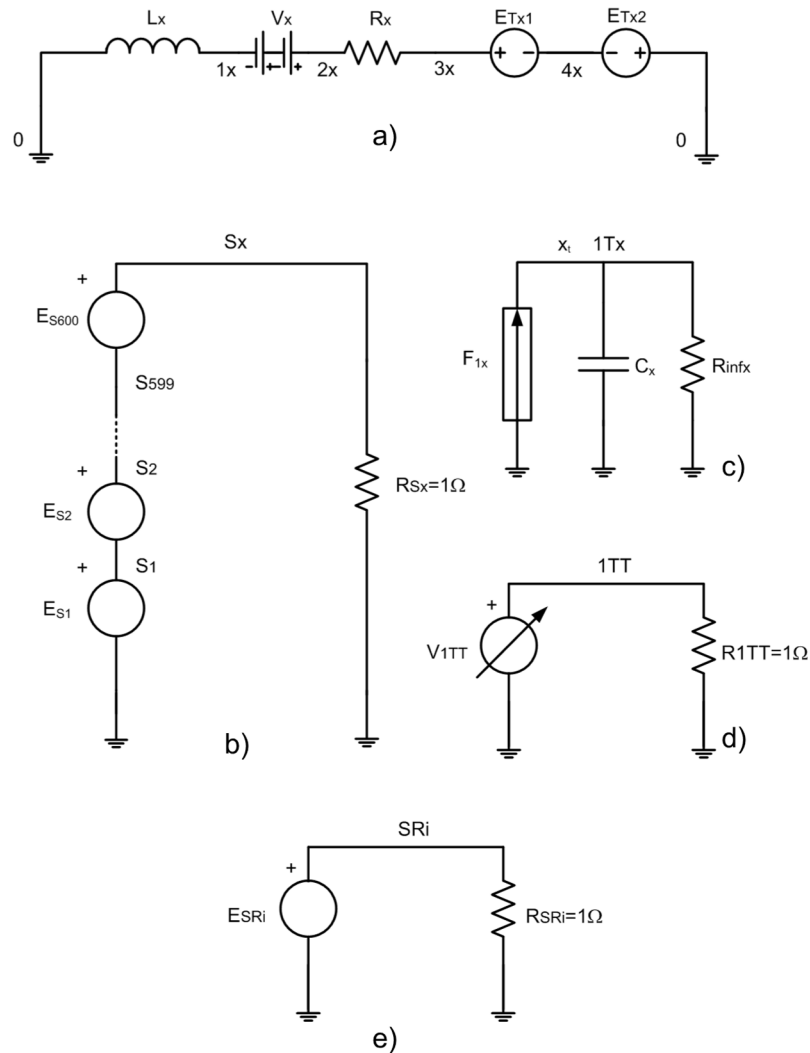


Fig 5. Network model of graphite with AFM. a) Main circuit, b) auxiliary circuit to get the force from Lennard-Jones potential, c) secondary circuit to get x_i , d) secondary circuit to the time, and e) secondary circuit to get the AFM tip and carbon atom distance.

<https://doi.org/10.1371/journal.pone.0193828.g005>

Firstly, the equivalence between the temperature or chemical concentration (oxygen concentration) and electrical variables: $c \equiv V_e$ (electric voltage) must be established.

Secondly, it is considered that the process advances parallel to the surface so it is only necessary to consider a dimension. Therefore, the material is discretized in one-dimensional cells, dividing the spatial variable x into n volume elements, Fig 6. Thus, the terms in second derivatives of the above equations can be expressed in finite differences by

$$\frac{\partial c_1(x, t)}{\partial t} = \frac{c_{1,x+\Delta x/2} - c_{1,x}}{\Delta x^2/2D_1} - \frac{c_{1,x} - c_{1,x-\Delta x/2}}{\Delta x^2/2D_1}; 0 < x < X(t) \tag{17}$$

$$\frac{\partial c_2(x, t)}{\partial t} = \frac{c_{2,x+\Delta x/2} - c_{2,x}}{\Delta x^2/2D_2} - \frac{c_{2,x} - c_{2,x-\Delta x/2}}{\Delta x^2/2D_2}; X(t) < x < \infty \tag{18}$$

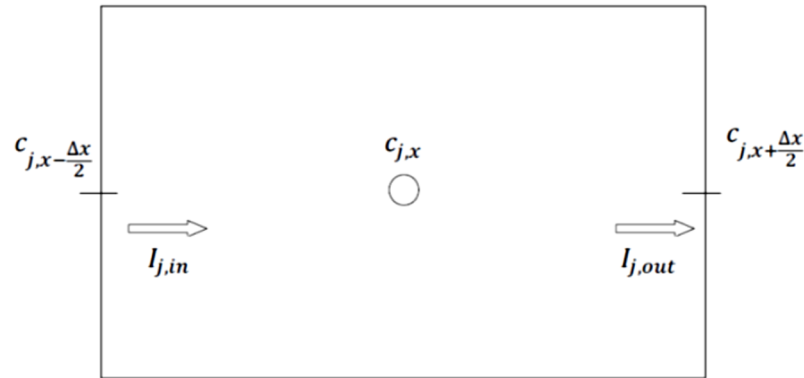


Fig 6. Nomenclature of the volume elements.

<https://doi.org/10.1371/journal.pone.0193828.g006>

Thirdly, the right terms of the Eqs (8) and (9), dc_j/dt are the currents that cross each capacitor, C_j . The voltage across each capacitor, $V_{C,j} = C_j^{-1} \cdot \int (d\theta_j/dt) dt$, is simply the variable c_j when $C_j = 1F$.

Fourthly, the Eq (10) gives the following differential finite difference equation:

$$-D_1 \frac{c_{1,x+\Delta x/2} - c_{1,x-\Delta x/2}}{\Delta x} + D_2 \frac{c_{2,x+\Delta x/2} - c_{2,x-\Delta x/2}}{\Delta x} - \Delta c \cdot \frac{dx}{dt} = 0 \quad (19)$$

The time derivative is discretized directly by the Spice Code Software tools [46,47], which automatically adjust the time increment to reach convergence more quickly. As mentioned with spatial discretization, the derivatives are associated with balances on the cell and not on each point of the mesh.

Fifthly, we proceed to the design of the network model. Fig 7 represents a cell inside the domain. In this circuit, each term, in Eqs (17) and (18), equal an electric current that is balanced with the current of another term in a common node.

The term on the left of the above equations, dc_j/dt , is the current across the capacitor C_j . The voltage in each capacitor, $V_{C,j} = C_j^{-1} \cdot \int (d\theta_j/dt) dt$ o $V_{C,y} = C_y^{-1} \cdot \int (dy/dt) dt$ is the variable c_j when $C_j = 1F$. Since there is a change of state in the cell, from metallic to oxidized, the capacitor used must have two different initial values, according to the state in which it is. In addition, with this software it is not possible to change the initial value of a capacitor, so it has been chosen to use two capacitors whose connection to the circuit is done through two switches controlled by voltage as indicated in Fig 7.

The last two linear terms of Eqs (17) and (18), $I_{j,in}$ and $I_{j,out}$, are represented as simple resistances, $R_{j,in}$ and $R_{j,out}$, respectively, since the equation of this electrical component is $i_R = V_R/R$. The resistance is $R_{j,in} = R_{j,out} = (\Delta x)^2/2D_j$. As mentioned, a change of state occurs in the cell, so the resistors used must have two different values. Since it is not possible to change these values with this software, it has been chosen to introduce, again, two resistors in parallel for each addition. An open switch disables the resistance in parallel, leaving only the resistance representing the initial state. When the switch is closed, two parallel resistors whose combined effect represents the final state are enabled, Fig 7.

Finally, each term in Eq (19) is considered a voltage equation and therefore a sequence of stresses that are introduced into the circuit by means of successive switches, allowing integrating the current position of the border, Fig 8 [44,45].

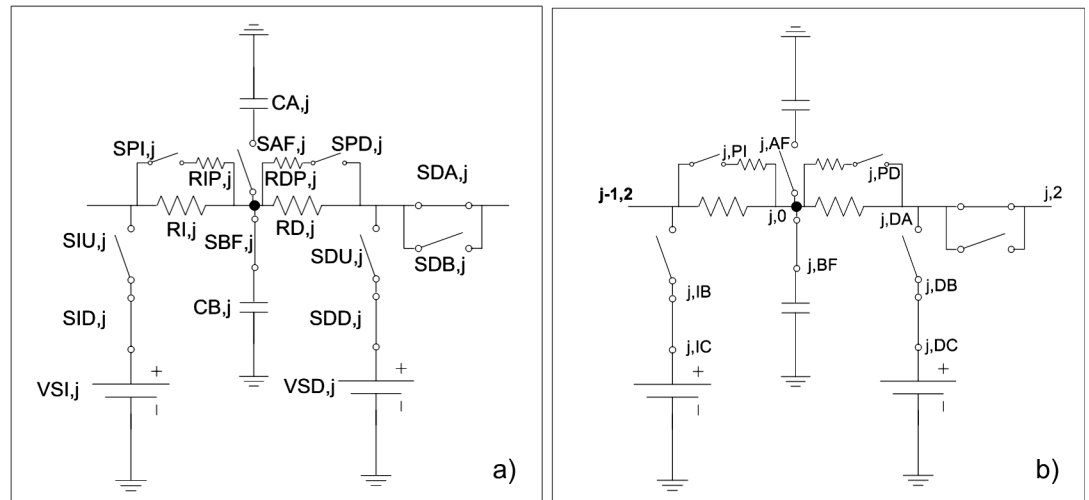


Fig 7. Equivalent electrical scheme of diffusion process in solid-liquid, liquid-solid or oxide-metal, system. a) circuit elements and b) nodes.

<https://doi.org/10.1371/journal.pone.0193828.g007>

4.3 Network model for the elastic problem

According to the NSM rules [1], the resulting cell is derived from the spatial discretization of the governing equation, Eq (14), and the adequate electro-mechanical analogy. One circuit is resultant from each differential equation. Thus, the resulting cell involves two circuits related to the unknowns u_x and u_y , respectively. Defining $C_1 = (\lambda + 2\mu)$, $C_2 = \mu$ and $C_3 = (\lambda + \mu)$, governing equation can be written in a more compact form:

$$\left. \begin{aligned} C_1 \frac{\partial^2 u_x}{\partial x^2} + C_2 \frac{\partial^2 u_x}{\partial y^2} + \left[C_3 \frac{\partial^2 u_y}{\partial x \partial y} + f_x \right] &= 0 \\ C_2 \frac{\partial^2 u_y}{\partial x^2} + C_1 \frac{\partial^2 u_y}{\partial y^2} + \left[C_3 \frac{\partial^2 u_x}{\partial x \partial y} + f_y \right] &= 0 \end{aligned} \right\} \quad (20)$$

Using the mesh and notation shown in Fig 9, each term in Eq (20) can be expressed in these finite differences:

$$\left. \begin{aligned} \frac{\partial^2 u}{\partial x^2} \Big|_{k,0} &\simeq \frac{\frac{u_{k,2} - u_{k,0}}{\Delta x/2} - \frac{u_{k,0} - u_{k,4}}{\Delta x/2}}{\Delta x} = \frac{u_{k,2} - 2u_{k,0} + u_{k,4}}{\Delta x^2/2} = - \left(\frac{u_{k,0} - u_{k,2}}{\Delta x^2/2} + \frac{u_{k,0} - u_{k,4}}{\Delta x^2/2} \right) \\ \frac{\partial^2 u}{\partial y^2} \Big|_{k,0} &\simeq \frac{\frac{u_{k,3} - u_{k,0}}{\Delta y/2} - \frac{u_{k,0} - u_{k,1}}{\Delta y/2}}{\Delta y} = \frac{u_{k,3} - 2u_{k,0} + u_{k,1}}{\Delta y^2/2} = - \left(\frac{u_{k,0} - u_{k,3}}{\Delta y^2/2} + \frac{u_{k,0} - u_{k,1}}{\Delta y^2/2} \right) \\ \frac{\partial^2 u}{\partial x \partial y} \Big|_{k,0} &\simeq \frac{\frac{u_{kt,2} - u_{kt,4}}{\Delta x} - \frac{u_{kb,2} - u_{kb,4}}{\Delta x}}{2\Delta y} = \frac{u_{kt,2} - u_{kt,4} - u_{kb,2} + u_{kb,4}}{2\Delta x \Delta y} \end{aligned} \right\} \quad (21)$$

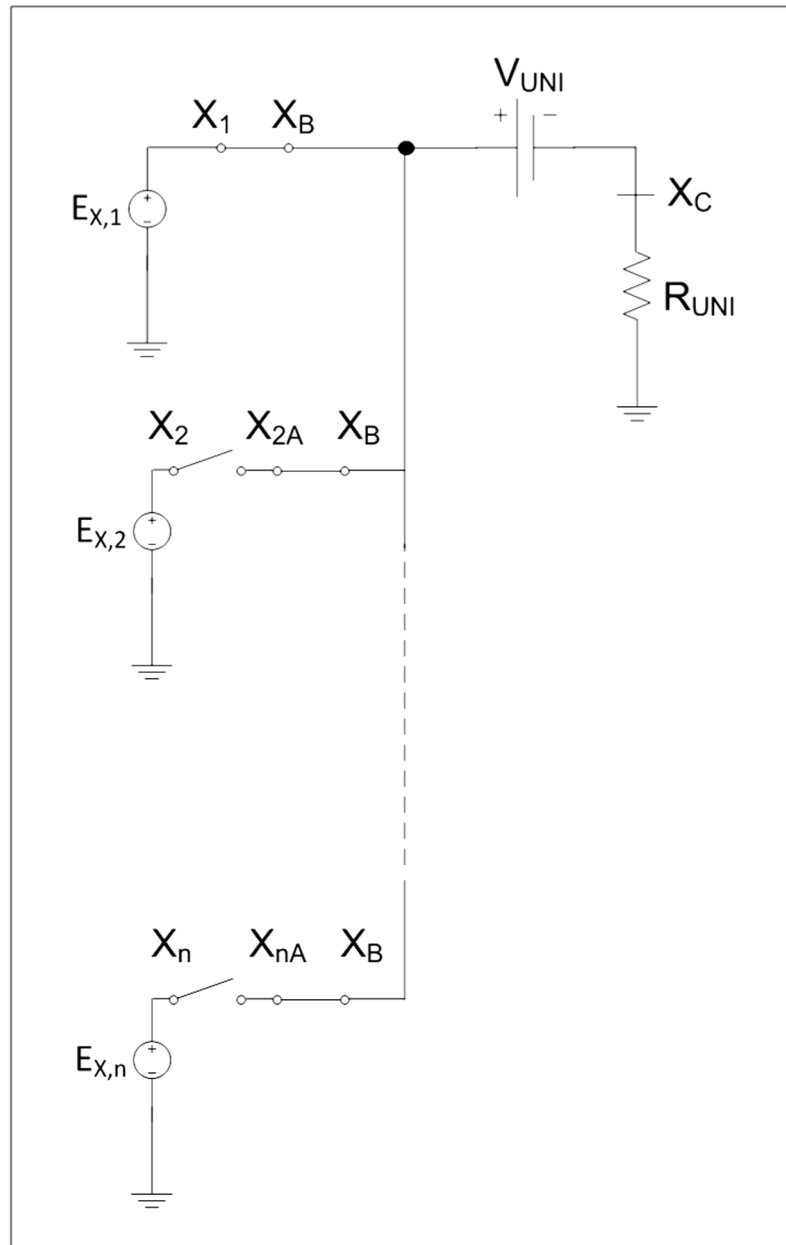


Fig 8. Network model of equilibrium equation.

<https://doi.org/10.1371/journal.pone.0193828.g008>

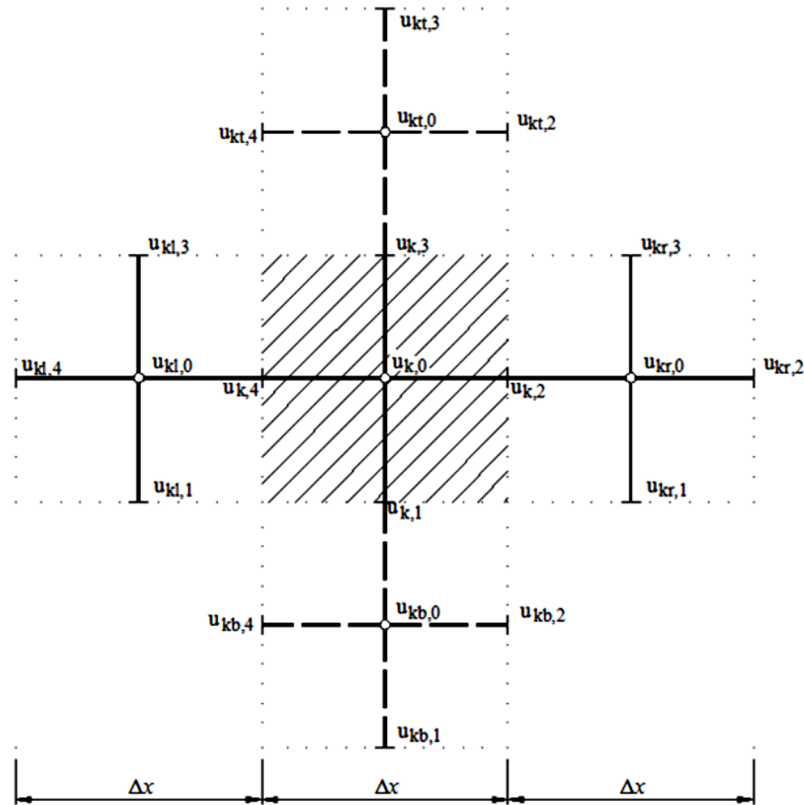


Fig 9. Mesh and notation.

<https://doi.org/10.1371/journal.pone.0193828.g009>

The resulting differences equations are:

$$\left. \begin{aligned} & \frac{u_{x_{k,0}} - u_{x_{k,2}}}{\left(\frac{\Delta x^2}{2}\right) \frac{1}{C_1}} + \frac{u_{x_{k,0}} - u_{x_{k,4}}}{\left(\frac{\Delta x^2}{2}\right) \frac{1}{C_1}} + \frac{u_{x_{k,0}} - u_{x_{k,3}}}{\left(\frac{\Delta y^2}{2}\right) \frac{1}{C_2}} + \frac{u_{x_{k,0}} - u_{x_{k,1}}}{\left(\frac{\Delta y^2}{2}\right) \frac{1}{C_2}} - \\ & \left[C_3 \frac{u_{y_{kt,2}} - u_{y_{kt,4}} - u_{y_{kb,2}} + u_{y_{kb,4}}}{2\Delta x \Delta y} + f_x \right] = 0 \\ & \frac{u_{y_{k,0}} - u_{y_{k,2}}}{\left(\frac{\Delta x^2}{2}\right) \frac{1}{C_2}} + \frac{u_{y_{k,0}} - u_{y_{k,4}}}{\left(\frac{\Delta x^2}{2}\right) \frac{1}{C_2}} + \frac{u_{y_{k,0}} - u_{y_{k,3}}}{\left(\frac{\Delta y^2}{2}\right) \frac{1}{C_1}} + \frac{u_{y_{k,0}} - u_{y_{k,1}}}{\left(\frac{\Delta y^2}{2}\right) \frac{1}{C_1}} - \\ & \left[C_3 \frac{u_{x_{kt,2}} - u_{x_{kt,4}} - u_{x_{kb,2}} + u_{x_{kb,4}}}{2\Delta x \Delta y} + f_y \right] = 0 \end{aligned} \right\} \quad (22)$$

Establishing the analogy between the mechanical displacement and electrical voltage, each equation shows a current balance. The resulting network model emerges from the electrical connection, in the whole domain $N_x \times N_y$, among the cells shown in Fig 10.

The model presents two coupled circuits: circuit 'ux' in corresponding with the rectangular u_x displacement and one more for the u_y component. Each cell contains the following components for circuits: four resistors corresponding with the primary four addends in both equations; values of the resistors are expressed in the denominator. In other hand, coupled terms between equations and volume forces (last addends in brackets), are implemented by using a voltage-controlled voltage-source.

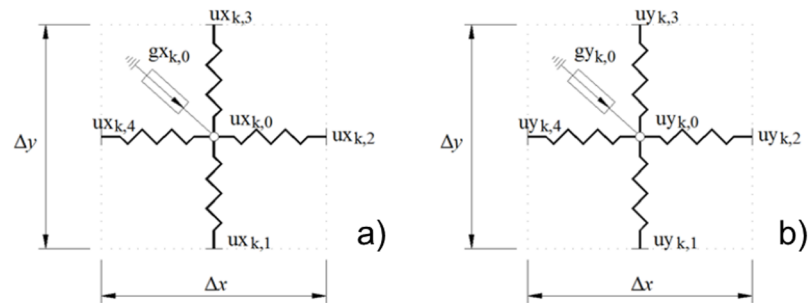


Fig 10. Cell of the network model. a) Circuit 'ux'; b) Circuit 'uy'.

<https://doi.org/10.1371/journal.pone.0193828.g010>

With regard to boundary conditions, while displacements are directly implemented by a constant voltage source, tractions, Eq (15), need the use of voltage-controlled voltage-sources.

5. Network models applications

5.1 Atomic-scale dry friction simulation: Atomic force microscopes network models

Network Simulation Method application of friction processes contained in the introduction is presented. For these processes, it is available partial results obtained by other authors with whom it is possible to verify the method. Furthermore, the effect of the parameters on the behavior of the proposed systems is discussed.

The NSM has been applied to studied surfaces and tips for which data are available: NaF and FFM tip [36], HOPG and SFM tip [37], and graphite and AFM tip [41].

5.1.1 Friction force microscope on a sodium fluoride surface simulation. The tip characteristics, the surface size and the test conditions for the tests selected are:

- The interaction between the NaF surface and the FFM tip is defined $m_x = m_y = 10^{-8}$ kg, $c_x = c_y = 10^{-3}$ N·s/m and $k_x = k_y = 10$ N/m. The tip support velocity is 400 Å/s, the scan range of 20x20 Å and the scan angle of 0° are used in order to show the results [36]. The potential defined in Eq (1) is used in the model represented by Eq (4).
- The interaction between the HOPG surface and the SFM tip is defined by $m_x = m_y = 10^{-8}$ kg, $c_x = c_y = 10^{-3}$ N·s/m and $k_x = k_y = 25$ N/m. The tip support velocity is 400 Å/s, the scan range of 20x20 Å and the scan angle of 7° are used in order to show the results [36]. The potential defined in Eq (1) is used in the model represented by Eq (4). The studied surface, with a very high stiffness [37], is integrated by 271 hexagons, defined by six carbon atoms (600 altogether).
- The interaction between graphite surface and the AFM tip is defined by $c_x = c_y = 0$ N·s/m, $k_x = k_y = 0.25-2.5$ N/m, $k_z = 0.25$ N/m, and a punching of -6 Å. The scan range of 9.8x8.5 Å and the scan angle of 15° are used in order to show the results [38]. Besides, $m_x = m_y = 10^{-6}$ kg and a tip support velocity of 10 Å/s, have been assumed in order to compare the results with Sasaki's ones [38].

The potential functions defined in the following equations are used in Eq (4):

- Eq (1) in the NaF surface and the FFM tip model
- Eq (2) in the HOPG surface and the SFM tip model
- Eq (3) in the graphite surface and AFM tip model

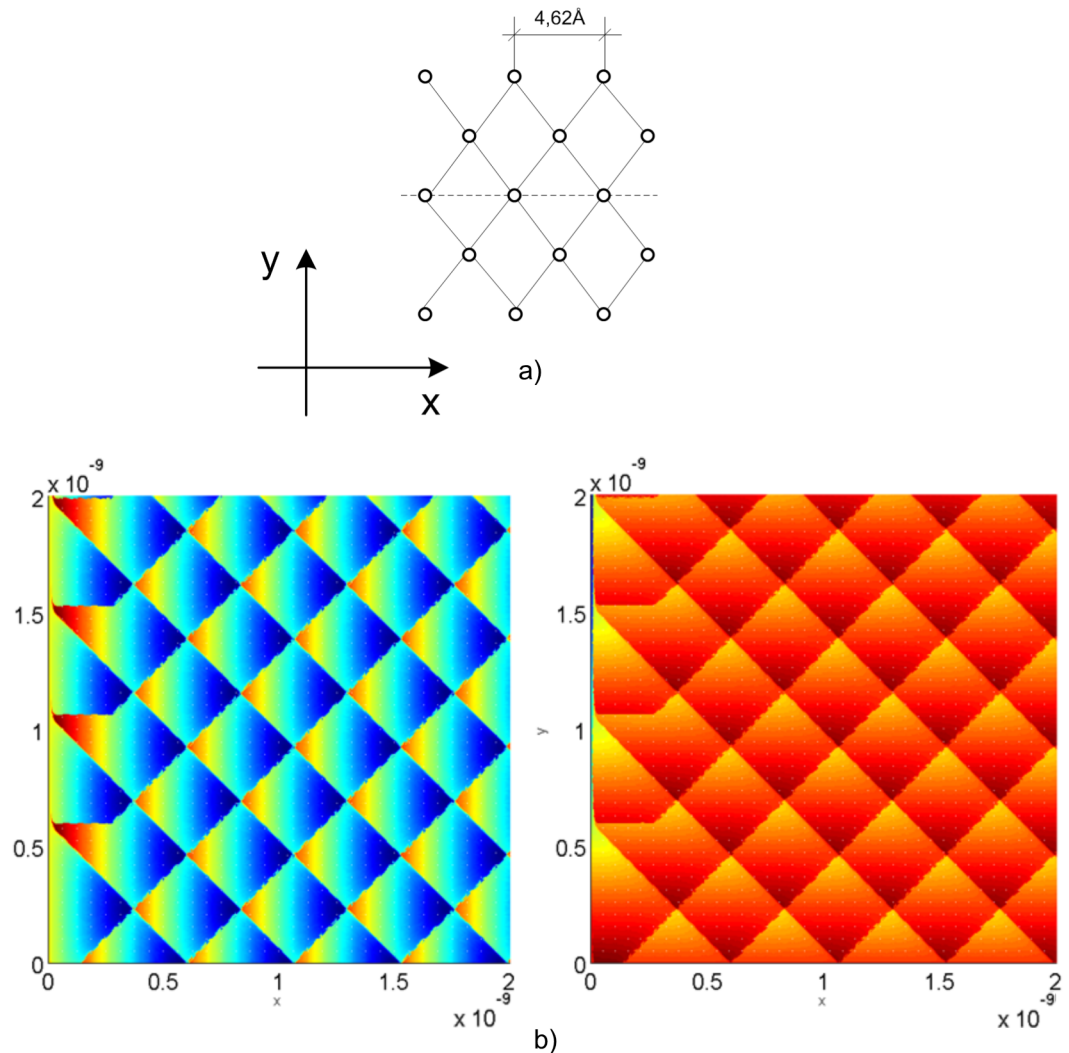


Fig 11. a) Position of the atoms in the NaF crystal net; b) Tip elastic force: F_x in the left and F_y in the right.

<https://doi.org/10.1371/journal.pone.0193828.g011>

In the last case, for graphite surface, the assumed model parameters are obtained using short computational time.

Fig 11(b) indicates the tip elastic force components, F_x and F_y , in each NaF surface position, whose crystal net is presented in Fig 11(a). The reciprocation between both represented images allows us to handle this code as an image interpretation tool from the microscope. Thus, this code is capable to handle a lot of crystal nets, even with crystallographic defects, providing the appropriate elastic forces, which could be contrasted with those from the microscope. The simulation results correspond to those accomplished by Hölscher et al. [36].

5.1.2 Atomic force microscope on a highly oriented pyrolytic graphite sample and on a graphite sample simulation. Fig 12(b) indicates the tip elastic force components, F_x and F_y , in each HOPG surface position, whose crystal net is presented in Fig 12(a). The simulation results correspond to those provided by Hölscher et al. [37]. Besides, Fig 13(b) shows the elastic force x-direction, F_x , in each position of the graphite surface, Fig 13(a). In this case, a 3D

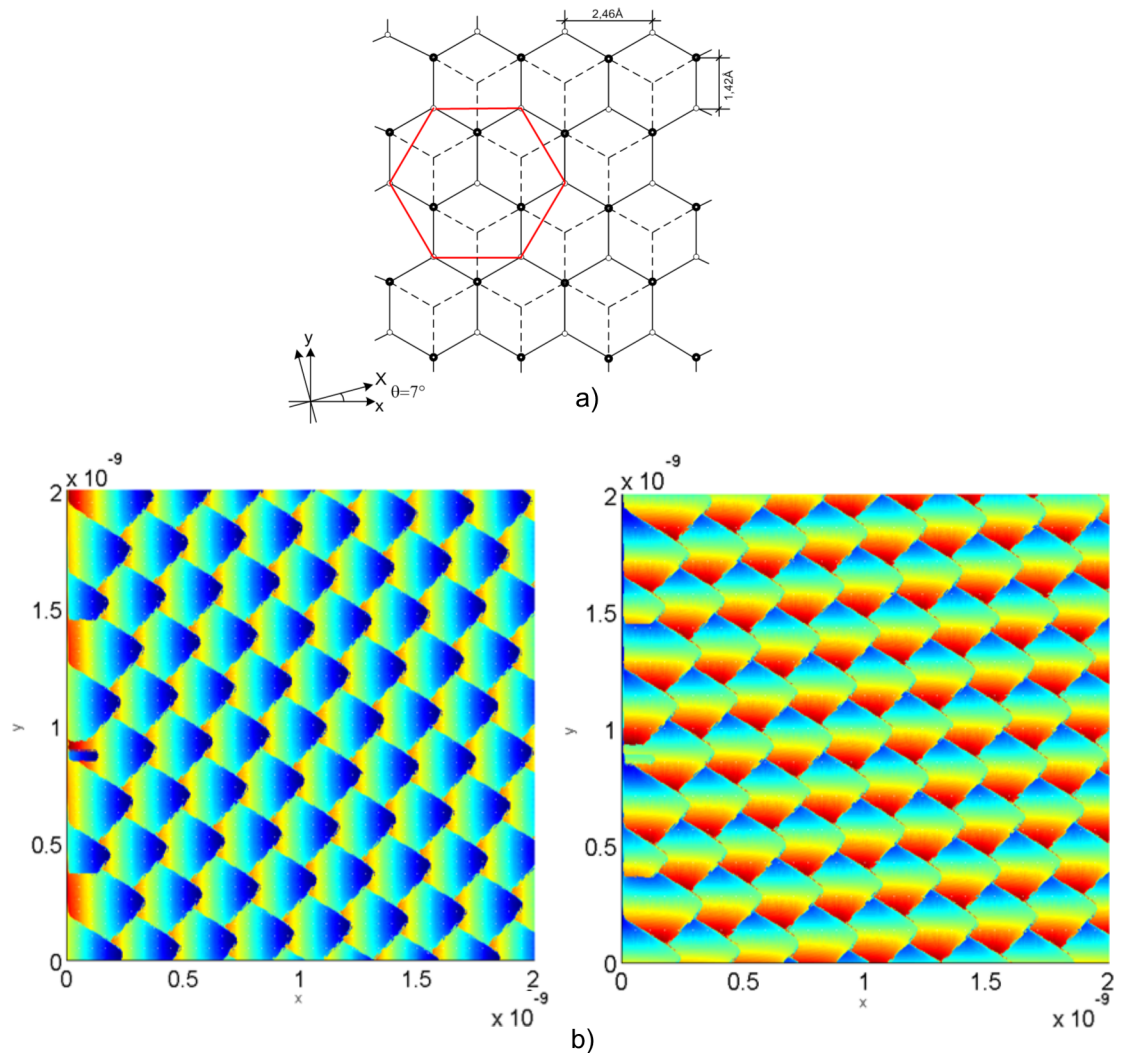


Fig 12. a) HOPG crystal net atoms position; b) Tip elastic force: F_x in the left and F_y in the right.

<https://doi.org/10.1371/journal.pone.0193828.g012>

plot is employed to depict the details better, specifically the stick-slip. The lines are plotted at different y-coordinates, separated by a fixed step. When one of these intersects the surface at a critical position, the instabilities appear, Fig 13(b). The simulation results correspond to those obtained by Sasaki et al. [38].

5.2 Moving corrosion fronts in titanium matrix composites

Lagoudas et al. [43] calculated the oxygen distribution throughout the oxide layer into the metal, assuming a rate position of the boundary between metal and oxide phases proportional to the square root of time. We solve this problem without making assumptions. In their analysis for SiC/Ti-15-3, used the values of diffusivity in the oxide, D_1 , and in the metal, D_2 , from the parameters of the Arrhenius equation, for temperatures between 600°C and 700°C, [39,48]. These parameters are shown in Table 1 [39,48–49].

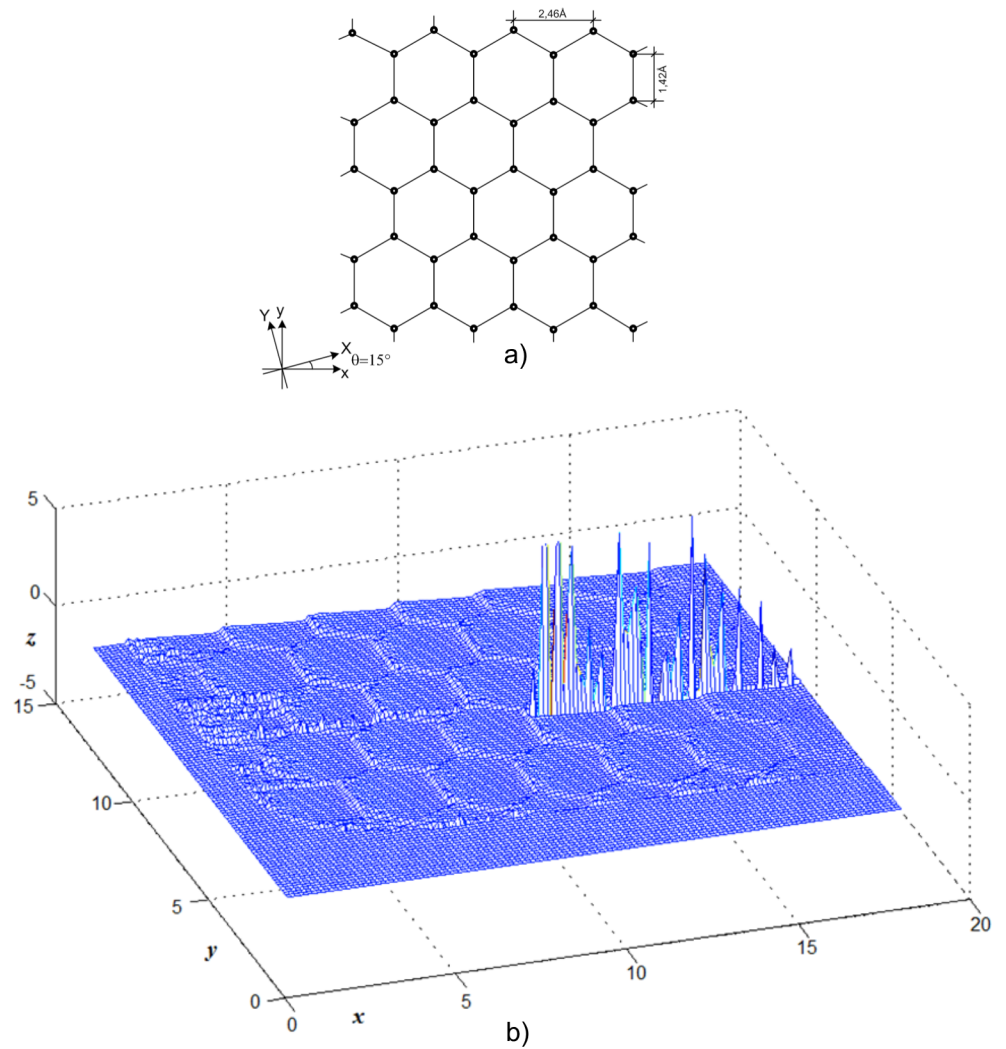


Fig 13. a) HOPG crystal net atoms position; b) Tip elastic force, F_x .

<https://doi.org/10.1371/journal.pone.0193828.g013>

Other authors, as Ariel et al. [49], estimate the diffusivity of oxygen in titanium 99.9% of purity, D_2 , using the parameters of the Arrhenius equation shown in the Table 1. We have used these parameters for modeling the oxidation of 99.9% pure titanium. Parameters of the oxide layer are the same as those used by Lagoudas *et al* [42,43]. The coefficients to calculate the diffusivity are defined in Table 1.

Table 1. Coefficients to calculate the diffusivity.

Species	A ($\mu\text{m}^2/\text{s}$)	E_a (cal/mol)
Metal (MMC)	$7.37 \cdot 10^6$	39960
Metal (Ti 99.9%)	17000	46062.1
Oxide	317.3	22756.2

<https://doi.org/10.1371/journal.pone.0193828.t001>

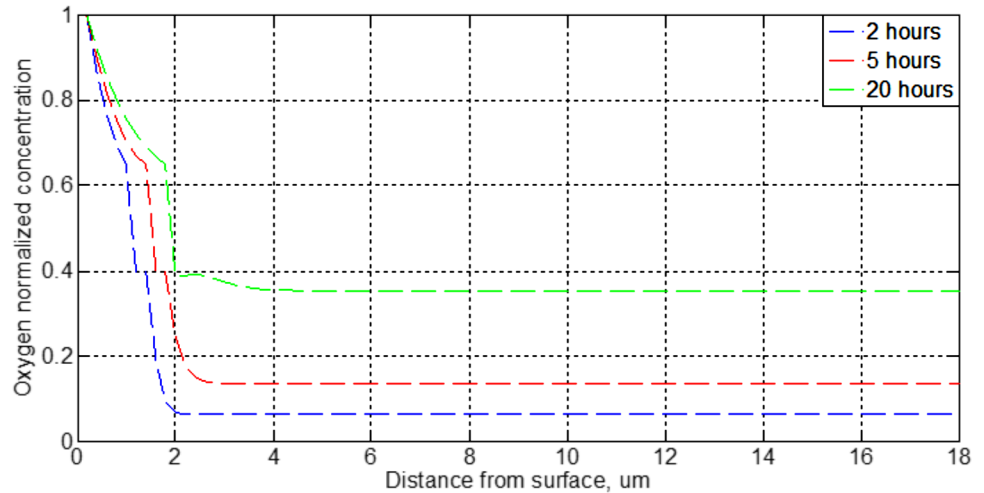


Fig 14. Distribution of oxygen concentration of the planar oxidation of Ti 99.9% for 2, 5 and 20 hours at 700°C.

<https://doi.org/10.1371/journal.pone.0193828.g014>

Fig 14 shows the results for Ti 99.9% for different time intervals. As immediate conclusion, we can observe the progressive slowing down of the progress of oxidation, because of achieving an oxide thickness of 2 μm takes around 20 hours.

If Fig 14 is compared with previous work [45], it can be seen that the matrix SiC/Ti 15-3 is oxidized at a faster rate than titanium 99.9%. The explanation is the higher oxygen diffusivity of the first material. As shown, the second material takes nearly 20 hours to achieve an oxide thickness of 2 μm.

Fig 15 shows as the progress of the oxidation frontier for a given temperature is stopped when it reaches a certain position, a determinate oxide thickness. After a time interval, the frontier advance is restarted. Furthermore, as expected, an increase in temperature reduces this interval. This figure shows a radically different behavior of matrix SiC/Ti-15-3 [45]. The explanation for this different behavior is due to a titanium diffusivity value lower in three orders of magnitude as the matrix SiC/Ti-15-3.

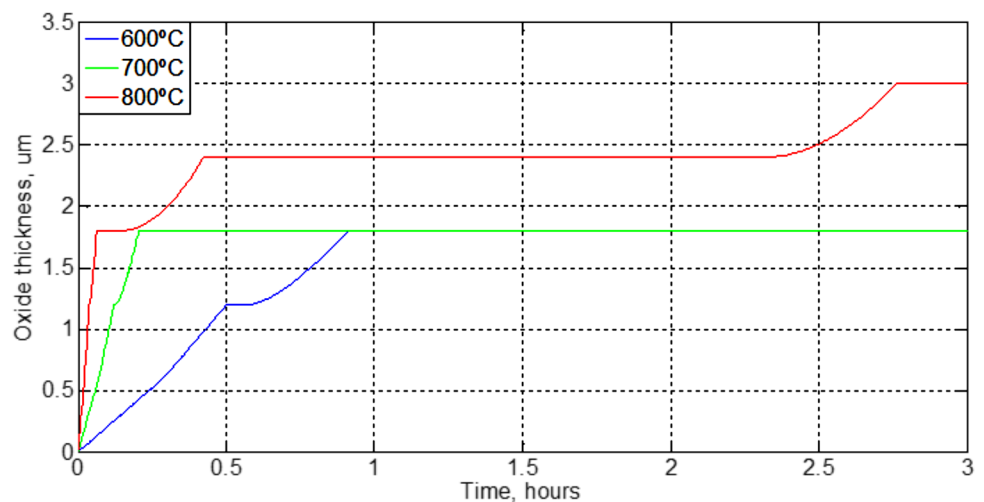


Fig 15. Evolution of interface at different temperatures of Ti 99.9%.

<https://doi.org/10.1371/journal.pone.0193828.g015>

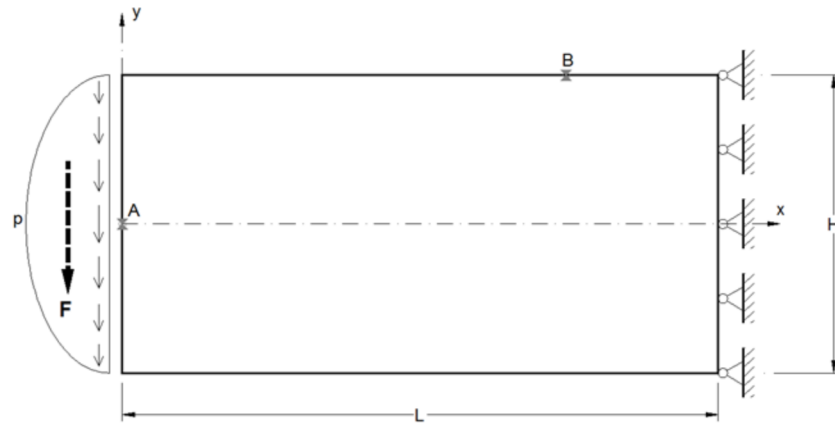


Fig 16. Cantilever beam subjected to shear loading.

<https://doi.org/10.1371/journal.pone.0193828.g016>

Fig 15 shows better the slowdown of corrosion at different temperatures. As expected with increasing temperature is an increase of the oxidation rate. These results are the same as those established for titanium alloys by ASTM B861-10 [50] and ‘Asociación de Investigación de la Rama Metalmeccánica de Valencia (AIMME)’ [51]. Their studies establish that the best alloys are those containing palladium and commercially pure titanium, 99.9%.

5.3 Cantilever beam subjected to shear loading

To show the applicability of the NSM in the elasticity field bending of a cantilever is solved for a rectangular cross section, Fig 16, Morales et al. [52]. This plane stress problem has been studied by Timoshenko & Goodier [53] under ideally boundary condition. The resultant shear force at the free end $F = 20 \cdot 10^3$ N is applied following a parabolic distribution according with the elementary strength material theory ($p = 30$ MPa). For the right end the boundary condition zero-displacement is imposed. Other geometric and material parameters are $L = 200$ mm, $H = 100$ mm, thickness = 10 mm, $\lambda = 121$ GPa and $\mu = 80$ GPa.

Fig 17 presents the results of the network simulation in term of the von Mises stress over the deformed domain draw with a scale factor of 50. Next figures (Figs 18 and 19) exhibit a

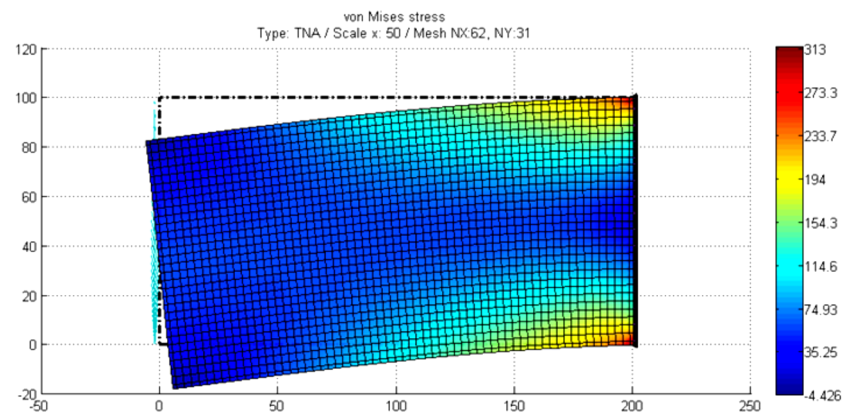


Fig 17. Von Mises stress in cantilever beam subjected to shear loading.

<https://doi.org/10.1371/journal.pone.0193828.g017>

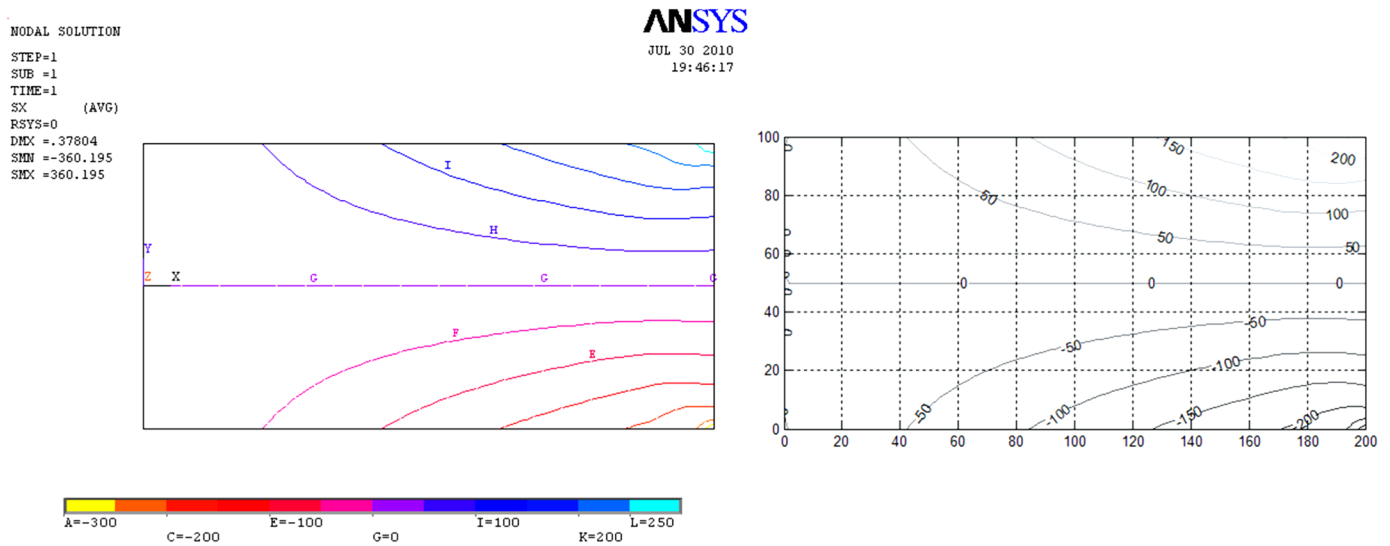


Fig 18. Stress isolines for the σ_{xx} component. Left: FEM solution. Right: NSM solution.

<https://doi.org/10.1371/journal.pone.0193828.g018>

comparison between NSM and FEM [54] numerical simulations in terms of u_x -displacement and σ_{xx} -stress. Fig 20 shows the vertical displacements at $y = 0$ for the analytical solutions studied by Timoshenko and Goodier (two ideal cases, Eqs n and r [53]), and the numerical solutions obtained by means of NSM and FEM for the boundary condition depicted in Fig 16. The numerical solutions of the deflection curves are very closed and bounded by the two analytical and ideal cases. Fig 21 shows the σ_{xx} -stress solutions for analytical and numerical methods for the upper edge line, $y = H/2$. These results are according to Saint-Venant's principle, where only significant differences can be appreciated near to the right section. For a better comparison, Table 2 details numerical results in points A, in the origin, and B, at 3/4 of L. (Fig 16).

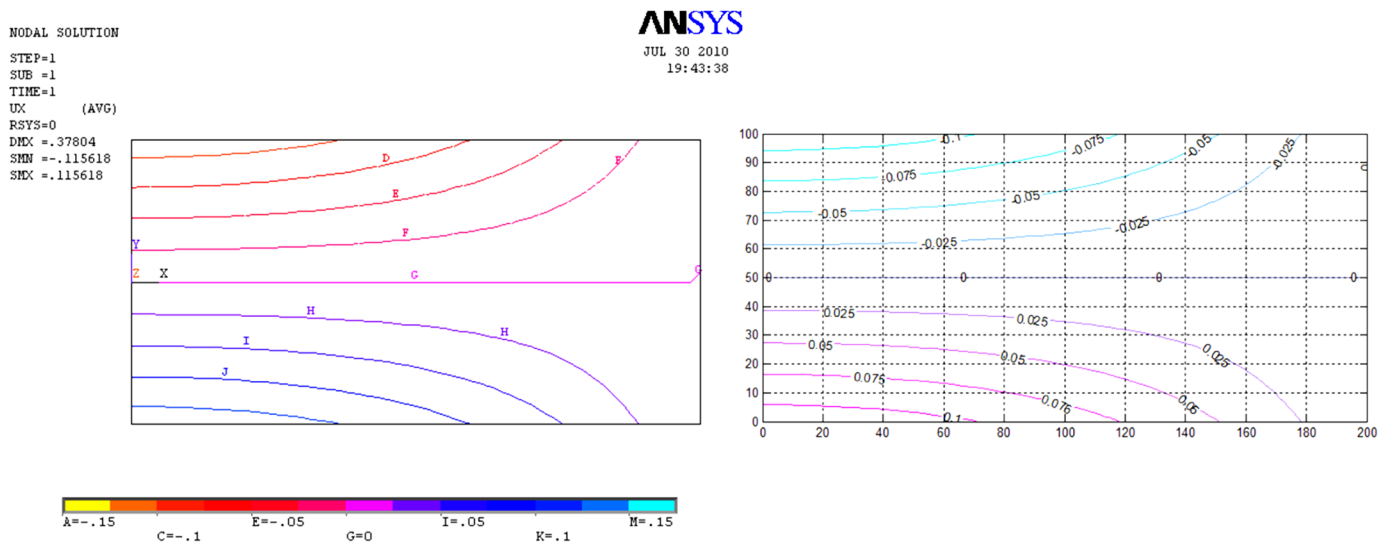


Fig 19. Displacement isolines u_x . Left: FEM solution. Right: NSM solution.

<https://doi.org/10.1371/journal.pone.0193828.g019>

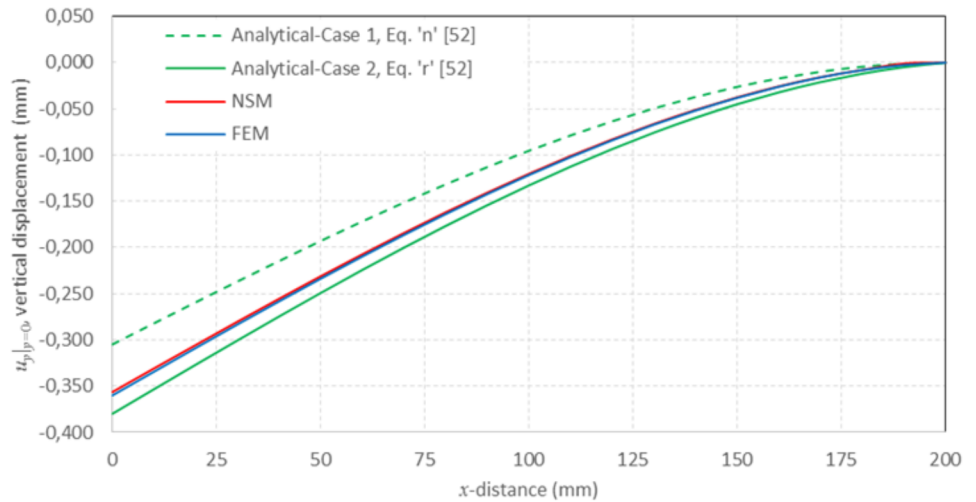


Fig 20. $u_y|_{y=0}$ vertical displacement for analytical, NSM and FEM solutions at $y = 0$.

<https://doi.org/10.1371/journal.pone.0193828.g020>

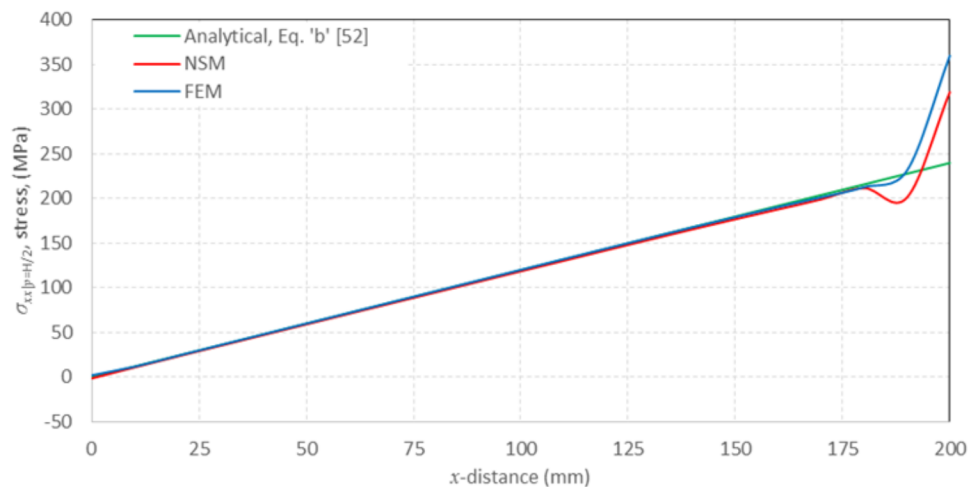


Fig 21. $\sigma_{xx}|_{y=H/2}$ normal stress component for analytical, NSM and FEM solutions at $y = H/2$.

<https://doi.org/10.1371/journal.pone.0193828.g021>

Table 2. Numerical results for FEM and NSM methods.

	FEM	NSM	Ratio	Deviation (%)
Point A: Deflection u_y , (mm)	-0.35995	-0.35620	0.9896	1.04
Point B: Stress σ_{xx} , (MPa)	-179.45	-177.07	0.9867	1.33

<https://doi.org/10.1371/journal.pone.0193828.t002>

6. Conclusions

Some numerical models based on the NSM have been designed and used—with negligible computing times in a suitable circuit simulation code—to successfully simulate different and representative engineering problems, such as dry friction in atomic scale, the moving front problems and elastic and solid mechanics, with no assumptions concerning the linearization

of the governing equations. The influence of the problems' main parameters is studied within a practical range of them. Comparison between the network model results and standard numerical methods or experimental data, which have been published in the scientific literature, confirms the reliability of the model.

Acknowledgments

We would like to thank Dr. González-Fernández, Emeritus Professor at the Universidad Politécnica de Cartagena, by the advancing of the pioneers and implementation of the NSM in Spain.

Author Contributions

Investigation: J. F. Sánchez-Pérez, F. Marín, J. L. Morales, M. Cánovas, F. Alhama.

Methodology: J. F. Sánchez-Pérez, F. Marín, J. L. Morales, M. Cánovas, F. Alhama.

Supervision: J. F. Sánchez-Pérez, F. Marín, M. Cánovas, F. Alhama.

Validation: J. F. Sánchez-Pérez, F. Marín, J. L. Morales, M. Cánovas.

Writing – original draft: J. F. Sánchez-Pérez, J. L. Morales, F. Alhama.

Writing – review & editing: J. F. Sánchez-Pérez, F. Marín, J. L. Morales, M. Cánovas, F. Alhama.

References

1. González-Fernández CF. Heat transfer and the network simulation method. In: Horno J, editor. Network Simulation Method. Research Signpost, Trivandrum, India; 2002. pp. 33–58.
2. Alarcón M. Transporte de calor en sistemas con aletas. Coeficientes de rendimiento y red de transferencia. Ph.D. Thesis, Universidad Politécnica de Cartagena. 2001. <https://dialnet.unirioja.es/servlet/tesis?codigo=49672>
3. Zueco J. Solución de problemas inversos en conducción de calor mediante el método de simulación por redes. Ph.D. Thesis, Universidad Politécnica de Cartagena. 2003. <http://repositorio.upct.es/handle/10317/794>
4. Castro E. Simulación de ondas elásticas en vigas mediante el método de redes y detección de daño mediante la transformada wavelet. Ph.D. Thesis, Universidad de Jaén. 2005. <http://hdl.handle.net/10481/604>
5. Soto A. Simulación numérica de procesos de intrusión salina en acuíferos mediante el método de simulación por redes. Ph.D. Thesis, Universidad Politécnica de Cartagena. 2007. <https://dialnet.unirioja.es/servlet/tesis?codigo=50096>
6. Del Cerro F. Desarrollo de un programa de conducción de calor, usando analogía eléctrica, mediante el lenguaje C# y el módulo de cálculo PSPICE. Aplicaciones lineales y no lineales en diferentes geometrías. Ph.D. Thesis, Universidad de Murcia. 2009. <http://hdl.handle.net/10201/31410>
7. Luna JP. Caracterización, optimización y diseño de algunos tipos de aletas a través del concepto de admitancia térmica inversa relativa. Ph.D. Thesis, Universidad Politécnica de Cartagena. 2010. <https://dialnet.unirioja.es/servlet/tesis?codigo=50119>
8. Alhama F, López-Sánchez JF, González-Fernández CF. Heat conduction through a multilayered wall with variable boundary conditions. *Energy*. 1997; 22(8): 797–803. [https://doi.org/10.1016/S0360-5442\(97\)00003-0](https://doi.org/10.1016/S0360-5442(97)00003-0)
9. González-Fernández CF, Alhama F, López-Sánchez JF, Horno J. Application of the network method to heat conduction processes with polynomial and potential-exponentially varying thermal properties. *Numerical Heat Transfer, Part A: Applications*. 1998; 33(5): 549–559. <https://doi.org/10.1080/10407789808913954>
10. Alarcón M, Alhama F, González-Fernández CF. Transient conduction in a fin-wall assembly with harmonic excitation—network thermal admittance. *Heat Transfer Engineering*. 2002; 23(2): 31–43. <https://doi.org/10.1080/01457630252800412>

11. Del Cerro F, Gómez-Lopera SA, Alhama F. A powerful and versatile educational software to simulate transient heat transfer processes in simple fins. *Computer Applications in Engineering Education*. 2008; 16(1): 72–82. <https://doi.org/10.1002/cae.20159>
12. Horno J, García-Hernández MT, González-Fernández CF. Digital simulation of electrochemical processes by the network approach. *Journal of Electroanalytical Chemistry*. 1993; 352(1–2): 83–97. [https://doi.org/10.1016/0022-0728\(93\)80256-H](https://doi.org/10.1016/0022-0728(93)80256-H)
13. Moya AA. Influence of DC electric current on the electrochemical impedance of ion-exchange membrane systems. *Electrochimica Acta*. 2011; 56(8): 3015–3022. <https://doi.org/10.1016/j.electacta.2010.12.103>
14. Horno J, González-Caballero F, Hayas A, González-Fernández CF. The effect of previous convective flux on the nonstationary diffusion through membranes network simulation. *Journal of Membrane Science*. 1990; 48(1): 67–77. [https://doi.org/10.1016/S0376-7388\(00\)80796-6](https://doi.org/10.1016/S0376-7388(00)80796-6)
15. Zueco J, Alhama F, González-Fernández CF. Inverse problem of estimating time-dependent heat transfer coefficient with the network simulation method. *Communications in Numerical Methods in Engineering*. 2005; 21(1): 39–48. <https://doi.org/10.1002/cnm.726>
16. Zueco J, Alhama F, González-Fernández CF. Inverse determination of heat generation sources in two-dimensional homogeneous solids: Application to orthotropic medium. *International Communications in Heat and Mass Transfer*. 2006; 33(1): 49–55. <https://doi.org/10.1016/j.icheatmasstransfer.2005.08.013>
17. Alhama I, Soto A, Alhama F. FATSIM-A: An educational tool based on electrical analogy and the code PSPICE to simulate fluid flow and solute transport processes. *Computer Applications in Engineering Education*. 2011; 16: 72–84. <https://doi.org/10.1002/cae.20577>
18. Zueco J, Alhama F. Simultaneous inverse determination of temperature-dependent thermophysical properties in fluids using the network simulation method. *International Journal of Heat and Mass Transfer*. 2007; 50(15–16): 3234–3243. <https://doi.org/10.1016/j.ijheatmasstransfer.2007.01.004>
19. Beg OA, Zueco J, Takhar HS, Bég TA, Sajid A. Transient nonlinear optically-thick radiative-convective double-diffusive boundary layers in a darcian porous medium adjacent to an impulsively started surface: network simulation solutions. *Communications in Nonlinear Science and Numerical Simulation*. 2009; 14(11): 3856–3866. <https://doi.org/10.1016/j.cnsns.2009.01.033>
20. Cánovas M, Alhama I, García G, Trigueros E, Alhama F. Numerical simulation of density-Driven flow and heat transport processes in porous media using the network method. *Energies*. 2017; 10(9): 1359. <https://doi.org/10.3390/en10091359>
21. Soto A, Alhama F, González-Fernández CF. An efficient model for solving density driven groundwater flow problems based on the network simulation method. *Journal of Hydrology*. 2007; 339(1–2): 39–53. <https://doi.org/10.1016/j.jhydrol.2007.03.003>
22. Alhama I, Soto A, Alhama F. Simulation of flow and solute coupled 2-D problems with velocity-dependent dispersion coefficient based on the network method. *Hydrological Processes*. 2012; 26(24): 3725–3735. <https://doi.org/10.1002/hyp.8457>
23. Alcaraz D, Alhama F, Moreno JA. Influence of fiber distribution in the thermal continuity of composites with titanium and magnesium alloys matrix (in Spanish). *Revista Española de Metalurgia*. 2005; Extr.: 293–303.
24. Moreno JA, Gómez FC, Alhama F. Solution of temperature fields in hydrodynamics bearings by the numerical network method. *Tribology International*. 2007; 40(1): 139–145. <https://doi.org/10.1016/j.triboint.2006.03.008>
25. Benavent A, Castro E, Gallego A. Evaluation of low-cycle fatigue damage in RC exterior beam-column subassemblages by acoustic emission. *Construction and Building Materials*. 2010; 24: 1830–1842. <https://doi.org/10.1016/j.conbuildmat.2010.04.021>
26. Marín F, Alhama F, Moreno JA. Modelling of stick-slip behaviour with different hypotheses on friction forces. *International Journal of Engineering Science*. 2012; 60: 13–24. <https://doi.org/10.1016/j.ijengsci.2012.06.002>
27. Morales JL, Moreno JA, Alhama F. New additional conditions for the numerical uniqueness of the Bousinesq and Timpe solutions of elasticity problems. *International Journal of Computer Mathematics*. 2012; 89(13–14): 1794–1807. <https://doi.org/10.1080/00207160.2012.667088>
28. Gómez-Lopera S, Alhama F, et al. PRODASIM: Programa de diseño de aletas simples. NAR 08/2005/544 [software]. Universidad Politécnica de Cartagena. 2005.
29. Alhama F, Del Cerro F. PROCCA: Programa de conducción de calor. NAR 08/2010/18 [software]. Universidad Politécnica de Cartagena. 2010.
30. Alhama I, Soto A, et al. FATSIM-A: Fluid flow and solute transport simulator. N. D. Mu-1093-2010 [software]. Universidad Politécnica de Cartagena. 2010.

31. Alhama I, Cánovas M, Alhama F. Simulation of fluid flow and heat transport coupled processes using FAHET software. *Journal of Porous Media*. 2015; 18(5): 537–546. <https://doi.org/10.1615/JPorMedia.v18.i5.60>
32. Morales JL, Moreno JA, Alhama F. EPSNET_10: Elasticity problems simulation network. NAR 08/2011/418 [software]. Universidad Politécnica de Cartagena. 2011.
33. Sánchez JF, Moreno JA et al. OXIPSIS_12: Oxidation processes simulation software. N. Mu-751-2013 [software]. Universidad Politécnica de Cartagena. 2013.
34. Peusner L. The principles of network thermodynamics: theory and biophysical applications. Entropy. Lincoln, USA; 1987.
35. Schwarz UD, Hölscher H. Atomic scale friction studies using scanning force microscopy. In: Bhushan B, editor. *Modern Tribology Handbook*, CRC Press, Boca Raton, Florida, USA; 2000. pp. 657–681.
36. Hölscher H, Schwarz UD, Wiesendanger R. Simulation of a scanned tip on a NaF(001) surface in friction force microscopy. *Europhysics Letters*. 1996; 36(1): 19–24. <https://doi.org/10.1209/epl/i1996-00181-4>
37. Hölscher H, Schwarz UD, Zwörner O, Wiesendanger R. Consequences of the stick-slip movement for the scanning force microscopy imaging of graphite. *Physical Review B*. 1998; 57(4): 2477–2481. <https://doi.org/10.1103/PhysRevB.57.2477>
38. Sasaki N, Kobayashi K, Tsukada M. Atomic-scale friction image of graphite in atomic-force microscopy. *Physical Review B*. 1996; 54(3): 2138–2149. <https://doi.org/10.1103/PhysRevB.54.2138>
39. Vuik C. Some historical notes about the Stefan problem. *Nieuw Archief voor Wiskunde, 4e serie* 11(2); 1993. pp. 157–167.
40. Barber JR. *Elasticity, Series: Solid Mechanics and its Applications*. vol. 172, 3rd ed. Springer. 2010.
41. Hölscher H, Allers W, Schwarz UD, Schwarz A, Wiesendanger R. Interpretation of "true atomic resolution" images of graphite (0001) in noncontact atomic force microscopy. *Physical Review B*. 2000; 62(11): 6967–6970. <https://doi.org/10.1103/PhysRevB.62.6967>
42. Ding Z, Lagoudas DC. A domain transformation technique in oxygen diffusion problems with moving oxidation fronts on unbounded domains. *International Journal of Numerical Methods in Engineering*. 1998; 42: 361–384. [https://doi.org/10.1002/\(SICI\)1097-0207\(19980530\)42:2<361::AID-NME377>3.0.CO;2-M](https://doi.org/10.1002/(SICI)1097-0207(19980530)42:2<361::AID-NME377>3.0.CO;2-M)
43. Lagoudas DC, Ma X, Miller DA, Allen DH. Modeling of oxidation in metal matrix. *International Journal of Engineering Science*. 1995; 33(15): 2327–2343. [https://doi.org/10.1016/0020-7225\(95\)00073-7](https://doi.org/10.1016/0020-7225(95)00073-7)
44. Sánchez JF. Solución numérica de problemas de oxidación mediante el método de simulación por redes. Ph.D. Thesis, Universidad Politécnica de Cartagena. 2012. <https://dialnet.unirioja.es/servlet/tesis?codigo=51906&orden=0&info=link>
45. Sánchez JF, Alhama F, Moreno JA. Numerical simulation of oxygen diffusion problems with moving oxidation fronts by network method. *International Review of Chemical Engineering (I.RE.CH.E.)*, Vol. 4, N. 6; Special Section on 4th International Conference on Chemical Engineering and Advanced Materials (CEAM) Virtual Forum. 2012; 4(6): 629–632.
46. Microsim Corporation Fairbanks PSpice 6.0, Irvine, California. 1994.
47. Nagel LW. SPICE2: A Computer Program to Simulate Semiconductor Circuits. University of California Berkeley; 1975.
48. Kofstad P. *High Temperature Oxidation of Metals*, 1st. ed. John Wiley & Sons, New York; 1966.
49. Ariel-Pérez R, Nakajima H, Dymont F. Diffusion in α -Ti and Zr. *Materials Transactions*. 2003; 44(1): 2–13. <https://doi.org/10.2320/matertrans.44.2>
50. ASTM B861-10 Standard Specification for Titanium and Titanium Alloy Seamless Pipe (Grades 1 to 38). Published online: <http://www.astm.org/Standards/B861.htm>.
51. Asociación de Investigación de la Rama Metalmeccánica de Valencia (AIMME). Estudio del empleo de nuevos materiales aplicaciones tradicionales de los fabricados. 2009.
52. Morales JL, Moreno JA, Alhama F. Numerical solutions of 2-D linear elastostatic problems by network method. *CMES-Computer Modeling Engineering Science*. 2011; 76(1): 1–18. <https://doi.org/10.3970/cmes.2011.076.001>
53. Timoshenko S, Goodier JN. *Theory of Elasticity*, 2nd. ed. New York: McGraw-Hill; 1951. pp. 35–39.
54. ANSYS, Inc.: ANSYS Release 9.0. ANSYS, Inc., Southpointe, 275 Technology Drive, Canonsburg, PA 15317, USA; 2004.